FKBP12 contributes to α-synuclein toxicity by regulating the calcineurin-dependent phosphoproteome

Gabriela Caraveo[a,1,2], Martin Soste[b], Valentina Cappelleti[b,c], Saranna Fanning[a], Damian B. van Rossum[d,e], Luke Whitesell[a], Yanmei Huang[a,3], Chee Yeun Chung[a,4], Valeriya Baru[a], Sofia Zaichick[f], Paola Picotti[b], and Susan Lindquist[a,g,h,5]

[a]Whitehead Institute for Biomedical Research, Cambridge, MA 02142; [b]Department of Biology, Institute of Biochemistry, Eidgenössische Technische Hochschule Zurich, 8092 Zurich, Switzerland; [c]Department of Computational Biology, Research and Innovation Centre, Foundation Edmund Mach, 38010 San Michele, Italy; [d]Department of Pathology, Penn State College of Medicine, Hershey, PA 17033; [e]The Jake Gittlen Laboratories for Cancer Research, Penn State College of Medicine, Hershey, PA 17033; [f]Department of Neurology, Feinberg School of Medicine, Northwestern University, Chicago, IL 60611; [g]Howard Hughes Medical Institute, Massachusetts Institute of Technology, Cambridge, MA 02139; and [h]Department of Biology, Massachusetts Institute of Technology, Cambridge, MA 02139

Calcineurin is an essential Ca²⁺-dependent phosphatase. Increased calcineurin activity is associated with α-synuclein (α-syn) toxicity, a protein implicated in Parkinson's Disease (PD) and other neurodegenerative diseases. Calcineurin can be inhibited with Tacrolimus through the recruitment and inhibition of the 12-kDa *cis-trans* proline isomerase FK506-binding protein (FKBP12). Whether calcineurin/FKBP12 represents a native physiologically relevant assembly that occurs in the absence of pharmacological perturbation has remained elusive. We leveraged α-syn as a model to interrogate whether FKBP12 plays a role in regulating calcineurin activity in the absence of Tacrolimus. We show that FKBP12 profoundly affects the calcineurin-dependent phosphoproteome, promoting the dephosphorylation of a subset of proteins that contributes to α-syn toxicity. Using a rat model of PD, partial elimination of the functional interaction between FKBP12 and calcineurin, with low doses of the Food and Drug Administration (FDA)-approved compound Tacrolimus, blocks calcineurin's activity toward those proteins and protects against the toxic hallmarks of α-syn pathology. Thus, FKBP12 can endogenously regulate calcineurin activity with therapeutic implications for the treatment of PD.

calcineurin | FKBP12 | α-synuclein | Parkinson's Disease | Tacrolimus

Calcium (Ca²⁺) homeostasis is critical for the cellular function of all living organisms. A key player in sensing Ca²⁺ concentrations and transducing this information into cellular responses is the highly conserved Ca²⁺–calmodulin-dependent phosphatase calcineurin (1). We recently reported that calcineurin regulates a tunable cellular response to α-synuclein (α-syn) (2), a small lipid binding protein involved in diverse synucleinopathies, such as Parkinson's Disease (PD) (3). High calcineurin activity drives a toxic response in the presence of high levels of α-syn. Conversely, reducing calcineurin activity with genetic tools or with Tacrolimus [a Food and Drug Administration (FDA)-approved drug also known as FK506] reduces the activity of the phosphatase, producing a protective outcome. Complete elimination of calcineurin activity, however, also leads to cell death (2).

For many decades, the prevailing model posits that calcineurin's mode of activation is dependent solely on Ca²⁺ and calmodulin (4, 5). A puzzling finding not easily accommodated in this model is that the natural compound Tacrolimus inhibits calcineurin through the formation of a ternary complex with 12-kDa *cis-trans* proline isomerase FK506-binding protein (FKBP12) (6). While there is some evidence that FKBP12 and calcineurin can interact physically in the absence of Tacrolimus (7–9), the physiologic relevance of this inhibitory complex is controversial and hence, has remained elusive. Despite this, there are indirect clues that FKBP12 and calcineurin may functionally interact within neuronal systems. Calcineurin is highly enriched in the brain (4) as is FKBP12, which has levels that are 50 times higher in the brain

than in any peripheral tissue (10). Moreover, the tissue distribution and subcellular localization of calcineurin closely resemble those of FKBP12 (11). Relevant to this study, calcineurin activity is increased in brain tissues from mice overexpressing α-syn and in humans afflicted with PD and other synucleinopathies (2, 12).

We reasoned that we could exploit the toxic effects of α-syn overexpression on calcineurin activation to interrogate whether FKBP12 plays a role in regulating calcineurin activity in the absence of Tacrolimus. Using a combination of genetic, pharmacologic, biochemical, and MS phosphoproteomic tools in diverse model systems, we find that FKBP12 modulates the calcineurin-dependent phosphoproteome, promoting the dephosphorylation of proteins involved in actin reorganization, ion channel regulation, endocytosis, and vesicle trafficking among others. Indeed, the trafficking of dopamine (DA) and dopamine transporters (DATs) is highly dependent on these very processes

Significance

Calcineurin is an essential Ca²⁺-dependent phosphatase in all eukaryotes. Whether calcineurin can be endogenously regulated by factors other than Ca²⁺ and calmodulin is not known. Using a model of Parkinson's Disease (PD) as a surrogate for high pathophysiological calcineurin activity and employing a shotgun proteomic approach, we show that the isomerase FKBP12 physiological regulates calcineurin activity by facilitating dephosphorylation of proteins involved in vesicle recycling. Using a rodent model of PD, partial inhibition of the functional interaction between FKBP12 and calcineurin blocks the phosphatase activity toward critical vesicle recycling proteins at nigral presynaptic terminals conferring strong neuroprotection. Our work reassigns to FKBP12 a novel mechanism that supports toxicity in a PD model by modulating calcineurin's phosphatase activity with therapeutic implications.

www.manaraa.com

and is severely affected in PD and in a rat model of α-syn toxicity (13). Within this rat model, partial reduction of calcineurin activity with low doses of Tacrolimus increased the phosphorylation of proteins, such as neuronal growth-associated protein 43 (GAP-43) and the Brain acid-soluble protein (BASP1), which have a critical role in restoring DA trafficking at the presynaptic terminals. Accordingly, this treatment rescued dopaminergic neurons from hallmark pathologies of PD as well as reversed a behavioral phenotype. Taken together, our data provide strong evidence that FKBP12 plays a major role in regulating calcineurin activity in the absence of Tacrolimus, thereby resolving the functional significance of Tacrolimus operating mode. Moreover, partial inhibition of the interaction between calcineurin and FKBP12, with low doses of the FDA-approved drug Tacrolimus, offers potential therapeutic implications for PD.

Results

Inhibition of FKBP12 Protects Against α-Syn Toxicity. Inducing the expression of human α-syn in yeast cells leads to cellular responses relevant to the α-syn–mediated pathologies observed in neurons. These include nitrosative stress (14, 15), defects in vesicle trafficking (16, 17), abnormal mitochondrial function (18), and Ca^{2+} dysregulation (2). In accord with our previous report (2), while in control experiments, concentrations of Tacrolimus did not affect the growth of non–α-syn–expressing yeast cells (Fig. S1A), intermediate concentrations of Tacrolimus rescue α-syn toxicity in yeast (Fig. 1A), in part by reducing calcineurin activation and converting an otherwise toxic response into a protective one. Cyclosporine A (CsA) is a structurally and functionally distinct calcineurin inhibitor that forms a repressive ternary complex between calcineurin and cyclophilin A (CyA), a *cis-trans* prolyl isomerase different from FKBP12, which is targeted by Tacrolimus. Unlike the yeast experiments with Tacrolimus, CsA did not reduce α-syn toxicity at any of the concentrations tested (Fig. 1B and Fig. S1B). One possibility for the lack of rescue might be the inability of CsA to accumulate in yeast cells. To test this, we challenged the survival of yeast cells in the presence of $MnCl_2$-induced stress, a calcineurin-dependent process (19). Survival in the presence of $MnCl_2$-induced stress was severely compromised in our control strain over a wide range of CsA concentrations (Fig. S1C). These experiments reveal that CsA penetrates yeast cells and inhibits calcineurin but does not rescue α-syn toxicity.

Next, we asked if the differential contribution of these calcineurin inhibitors to α-syn toxicity was conserved in mammalian neurons. For these experiments, we used embryonic rat cortical neurons infected with a lentivirus carrying the disease-associated mutation of α-syn, A53T (20). These neurons are more abundant than highly vulnerable dopaminergic neurons and are also affected in patients with PD (21). In agreement with our yeast data, intermediate, subsaturating concentrations of Tacrolimus rescued neurons from the toxic effect of α-syn expression assessed by an ATP assay as well as by counting the remaining MAP2-positive neurons in the well (Fig. 1 C and E). Higher concentrations of Tacrolimus, which completely inhibit calcineurin, were not protective and in fact, increased toxicity. In control experiments, these concentrations did not compromise the viability of neurons not expressing α-syn (Fig. S1D). In addition, we found that the bell-shaped curve of Tacrolimus rescue was observed even at higher levels of α-syn toxicity (Fig. S1E). Importantly, the differences in calcineurin activation between control and α-syn–expressing neurons were not caused by differences in calcineurin expression but rather, calcineurin activity (Fig. S1F).

Consistent with results in yeast, at concentrations where neuronal viability was not compromised (Fig. S1G) and irrespective of the extent of α-syn toxicity, CsA did not rescue. In fact, CsA enhanced α-syn toxicity at concentrations of 1 μM assessed by an ATP assay as well as by counting the remaining MAP2-positive neurons in the well (Fig. 1 D and E). Since CsA and Tacrolimus

directly interact with distinct prolyl isomerases to inhibit calcineurin, these observations suggest that FKBP12 plays an important and specific role in modulating α-syn toxicity.

To further test this hypothesis, we individually deleted each member of the FKBP and cyclophilin gene families in yeast (this experiment is difficult to interpret in mammalian cells, since deletion of some of the FKBP and cyclophilin members is embryonic lethal). These deletions had no effect on viability of yeast cells in the absence of α-syn (Fig. 1F) in accord with previous studies (22). Remarkably, deletion of the yeast FKBP12 gene (FPR1) and to a lesser extent, the closely related yeast FKBP13 gene (FPR2) conferred protection against α-syn toxicity (Fig. 1F). In contrast, deletion of the yeast CyA gene (CPR1) actually enhanced α-syn toxicity (Fig. 1F). Deletion of other members of the FKBP and cyclophilin families either had no effect (cpr 4, 5, 7, and 8) or increased toxicity (cpr 2, 3, and 6) (Fig. 1F). These genetic experiments mirror the pharmacological data and indicate that CyA plays a protective role, whereas FKBP12 contributes to α-syn toxicity.

Inhibition of FKBP12 Confers Protection Against α-Syn Toxicity Through Calcineurin-Dependent and -Independent Pathways. We previously showed that calcineurin activity is a critical determinant of α-syn toxicity (2). In this report, our data suggest that FKBP12 is also a critical mediator of α-syn toxicity based on the protection afforded by genetic deletion of FKBP12 as well as the rescue of toxicity by Tacrolimus but not CsA. To investigate whether the neuroprotective properties of low doses of Tacrolimus against α-syn toxicity are caused by inhibition of FKBP12 and/or calcineurin, we took a genetic, pharmacological, and biochemical approach.

Deletion of calcineurin's regulatory subunit, Cnb1p, eliminates calcineurin function in yeast without affecting the growth in the absence of α-syn (Fig. 2A and Fig. S2). The deletion also has little net effect on α-syn toxicity. Conversely, the deletion of the yeast FKBP12 conferred strong protection against α-syn toxicity. Importantly, the double deletion of calcineurin and FKBP12 markedly reduced, although did not completely eliminate, the protective effects of the FKBP12 deletion (Fig. 2A and Fig. S2). This result suggests that FKBP12 contributes to α-syn toxicity in a calcineurin-dependent as well as a calcineurin-independent manner.

To further dissect the relationship between these two proteins, we took advantage of the binding mode of the pharmacological agent Tacrolimus. One side of Tacrolimus binds to the catalytic pocket of FKBP12 and inhibits its ability to catalyze *cis-trans* isomerization of proline amino acids. The other side of Tacrolimus forms a composite surface with FKBP12 and calcineurin, thus inhibiting the phosphatase in a noncompetitive manner (23). Therefore, while Tacrolimus can inhibit FKBP12 in the absence of calcineurin, calcineurin can only be inhibited by Tacrolimus in the presence of FKBP12. We reasoned that we could determine the contribution of each protein to this inhibitory activity if we deleted calcineurin and FKBP12, individually and in combination, in the α-syn–expressing yeast strain and assess growth over a broad range of Tacrolimus doses.

In cells carrying the calcineurin deletion (calcineurin KO), Tacrolimus provided substantial but not full rescue at all concentrations tested (Fig. 2 B and C). Importantly, Tacrolimus can still inhibit FKBP12 in these calcineurin-deleted cells, thereby conferring some protective effect. This fact suggests that FKBP12 can exert some of its toxic effects independent of calcineurin. Conversely, KO of FKBP12 (FKBP12 KO) produced substantial rescue in the presence of calcineurin (Fig. 2D). This was not affected by the addition of Tacrolimus at any concentration, showing that the protective effects of Tacrolimus require the presence of FKBP12 and are not caused by off-target effects. Notably, the deletion of FKBP12 did not produce the optimal rescue effect of Tacrolimus observed in WT α-syn–expressing cells (Fig. 2 B and D). These data suggest that the maximal protective effects of Tacrolimus against α-syn toxicity are achieved by partial inhibition of both calcineurin and FKBP12. To confirm this possibility, we tested the effect of the
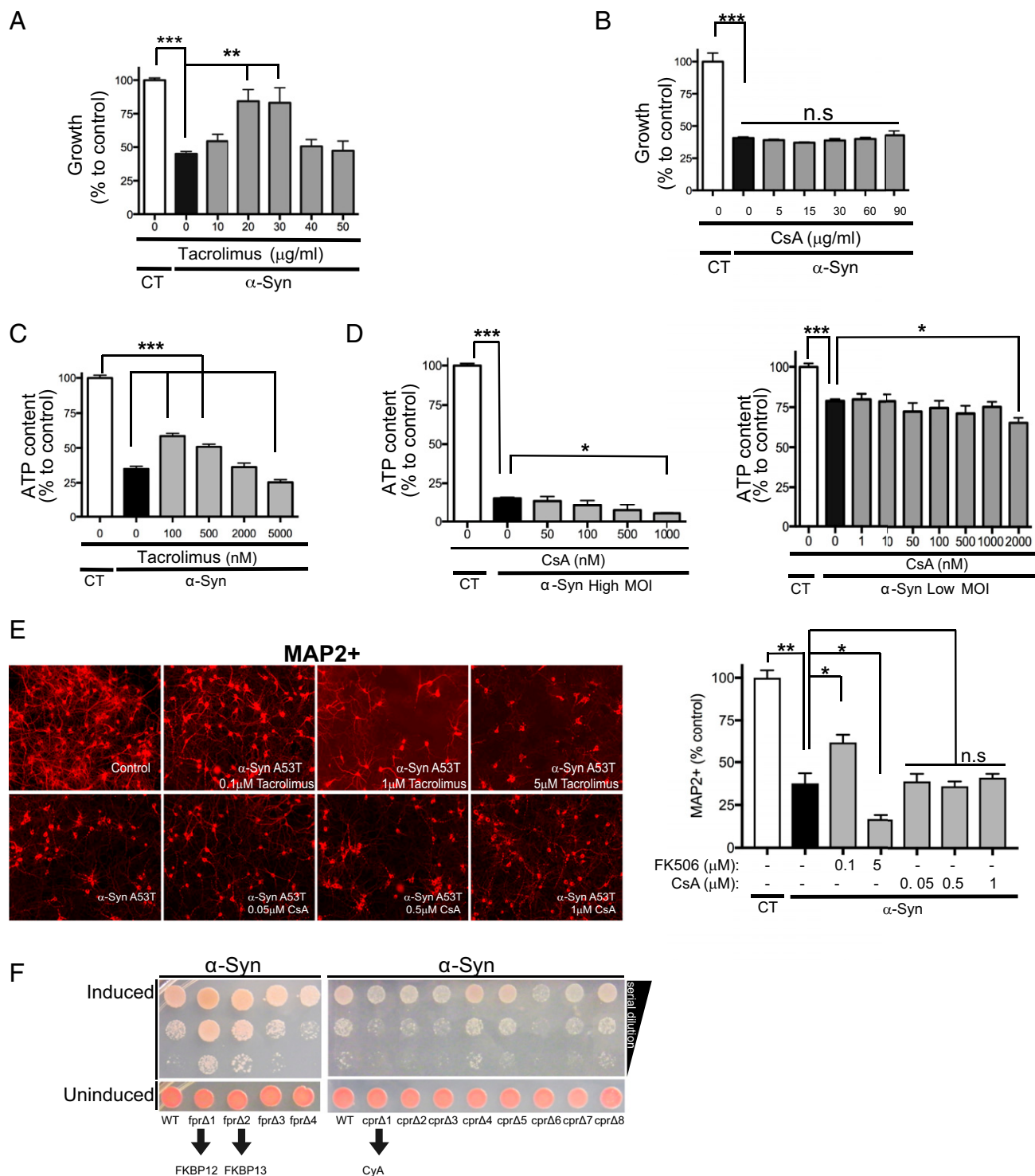
www.manaraa.com

Fig. 1. Inhibition of FKBP12 protects against α-syn toxicity. (*A*) Growth [described as percentage of control (CT)] of α-syn–expressing yeast cells grown for 48 h over a range of Tacrolimus concentrations. **$P < 0.005$ (one-way ANOVA, Fisher's test); ***$P < 0.0005$ (one-way ANOVA, Fisher's test). (*B*) Growth [described as percentage of control (CT)] of α-syn–expressing yeast cells grown for 48 h at the indicated CsA concentrations. ***$P < 0.0005$ (one-way ANOVA, Fisher's test). (*C*) Rat cortical neurons infected with high-titer (high MOI) α-syn and/or LacZ as control (CT) treated with vehicle and/or increasing concentrations of Tacrolimus for 14 d and assayed for ATP content as a surrogate for viability. ***$P < 0.005$ (one-way ANOVA, Fisher's test). (*D*) Same as in *C*, but neurons were infected with low titer (low MOI) and high titer (high MOI) of α-syn A53T and treated with various concentrations of CsA. Neuronal experiments performed in *C* and *D* represent data from six replicates in three independent experiments. The SE is present; it is very low. *$P < 0.05$ (one-way ANOVA, Dunnett's multiple comparison test); ***$P < 0.0005$ (one-way ANOVA, Dunnett's multiple comparison test). (*E*) Representative images of neuronal microtubule 2 (MAP2) red staining of rat primary neuronal cultures infected with either control lentivirus LacZ (control) and high-MOI α-syn A53T treated with various doses of FK506 or CsA for 14 d. Percentages of MAP2-positive neurons relative to control (LacZ infected) in the conditions described in *C* and *D*. *$P < 0.05$ (one-way ANOVA, Dunnett's multiple comparison test); **$P < 0.005$ (one-way ANOVA, Fisher's test). (*F*) α-Syn–expressing yeast cells lacking individual FKBPs (*fpr1-4Δ*) and cyclophilins (*cpr1-8Δ*) were spotted onto plates containing uninducing media (SD−His,Trp−α-syn selective; *Lower*) and replica plated in threefold serial dilutions on α-syn–inducing plates containing selective media SGal (*Upper*). All yeast experiments were performed in triplicate with at least three biological replicates each time. n.s, nonsignificant; MOI, multiplicity of infection; SGal, synthetic galactose.
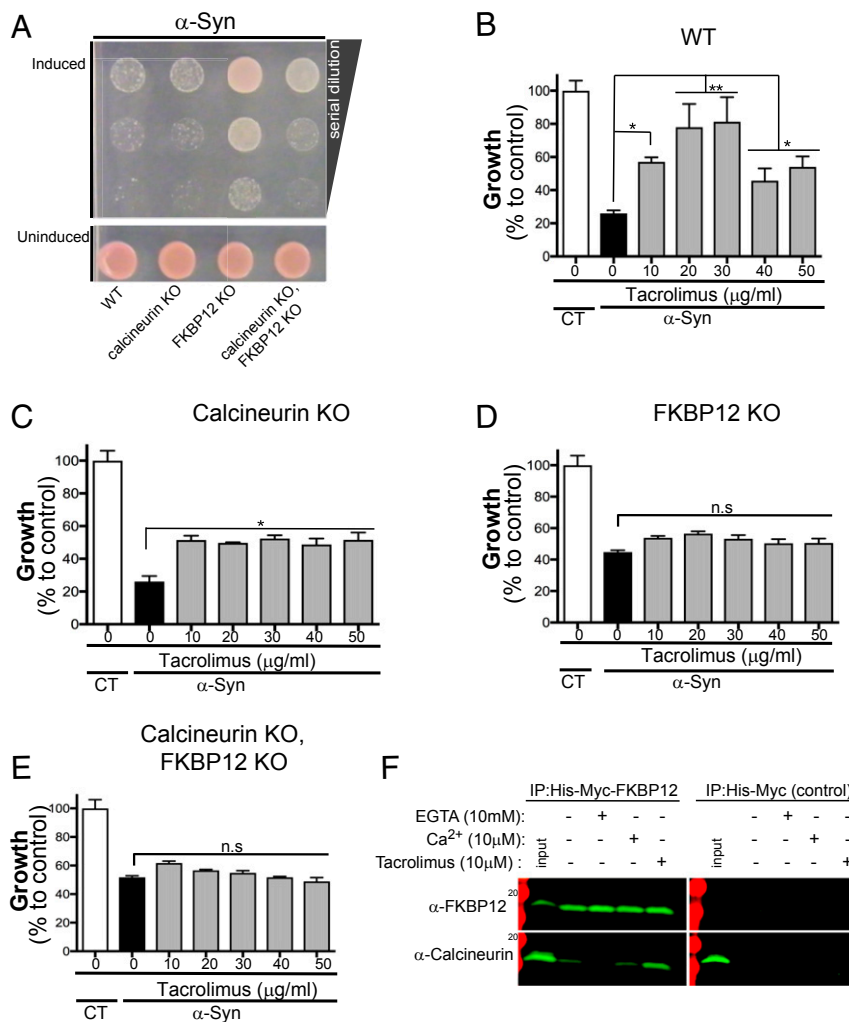
Caraveo et al.

Fig. 2. FKBP12 protects against α-syn toxicity in calcineurin-dependent and -independent manners. (*A*) α-Syn–expressing yeast cells either WT or lacking yeast FKBP12, *fpr1* (FKBP12 KO); yeast calcineurin, *cnb1* (calcineurin KO); or both yeast FKBP12 and calcineurin (calcineurin KO, FKBP12 KO) were spotted onto plates containing uninducing media (SD–His,Trp–α-syn selective; *Lower*) and replica plated in threefold serial dilutions on α-syn–inducing plates containing selective media synthetic galactose (SGal) (*Upper*). (*B–E*) Growth (described as percentage over control) of α-syn–expressing yeast cells: WT (*B*), lacking yeast calcineurin (calcineurin KO; *C*), lacking yeast FKBP12 (FKBP12 KO; *D*), or lacking both FKBP12 and calcineurin (FKBP12 KO and calcineurin KO; *E*). Cells were grown for 48 h over a range of Tacrolimus concentrations. All yeast experiments were performed in triplicates with at least three biological replicate each time. All statistical comparisons were performed relative to no drug within each of the genetic conditions. *$P < 0.05$ (one-way ANOVA, Dunnett's multiple comparison test); **$P < 0.005$ (one-way ANOVA, Dunnett's multiple comparison test). (*F*) HEK 293 cells were stably transfected with His-Myc-FKBP12 and/or His-Myc, lysed, and treated with EGTA (10 mM), CaCl (10 μM), and/or Tacrolimus (10 μM). Lystes were subsequently immunoprecipitated (IP) with nickel beads and probed for calcineurin (α-CNB) and/or FKBP12 (α-Myc) by Western blot.

calcineurin and FKBP12 double deletion in α-syn–expressing yeast cells. The double deletion conferred some but not full protection against α-syn toxicity, and this rescue was not affected by Tacrolimus (Fig. 2 *B* and *E*). These pharmacological and genetic findings reveal a physiological interaction between calcineurin and FKBP12 largely responsible for the toxic effects of α-syn. To determine whether calcineurin and FKBP12 can physically interact in the absence of Tacrolimus, we turned to a mammalian system. Indeed, in HEK 293 cells, calcineurin can interact with FKBP12 in the absence of Tacrolimus (Fig. 2*F*). As previously reported, addition of Tacrolimus enhances this interaction by stabilizing while inhibiting the enzymatic properties of both enzymes (Fig. 2*F*). However, addition of the Ca^{2+} chelator EGTA disrupts the endogenous interaction between calcineurin and FKBP12, suggesting that this interaction occurs under high Ca^{2+}, such as the conditions triggered by α-syn.

Together, these genetic, pharmacological, and biochemical findings establish that FKBP12 can interact with calcineurin in

the absence of Tacrolimus and contribute to α-syn toxicity in a calcineurin-dependent pathway.

FKBP12 Modulates the Calcineurin-Dependent Phosphoproteome. FKBP12 has been shown to play a pathological role in α-syn toxicity, which is independent of calcineurin (24). This is in agreement with our pharmacological and genetic data; however, our findings also support the notion that FKBP12 contributes to α-syn toxicity through a calcineurin-dependent mechanism. This suggests that FKBP12 could exert part of its toxic effects by modulating calcineurin function. Phosphatases exert their effects by dephosphorylating substrates, which ultimately results in the activation and/or repression of downstream pathways. If FKBP12 contributes to α-syn toxicity by enabling calcineurin to dephosphorylate substrates, with dephosphorylation that contributes to cell death, we reasoned that inhibition of the functional interaction between FKBP12 and calcineurin should restore the phosphorylation state of those substrates. In doing so, this restoration may confer protection
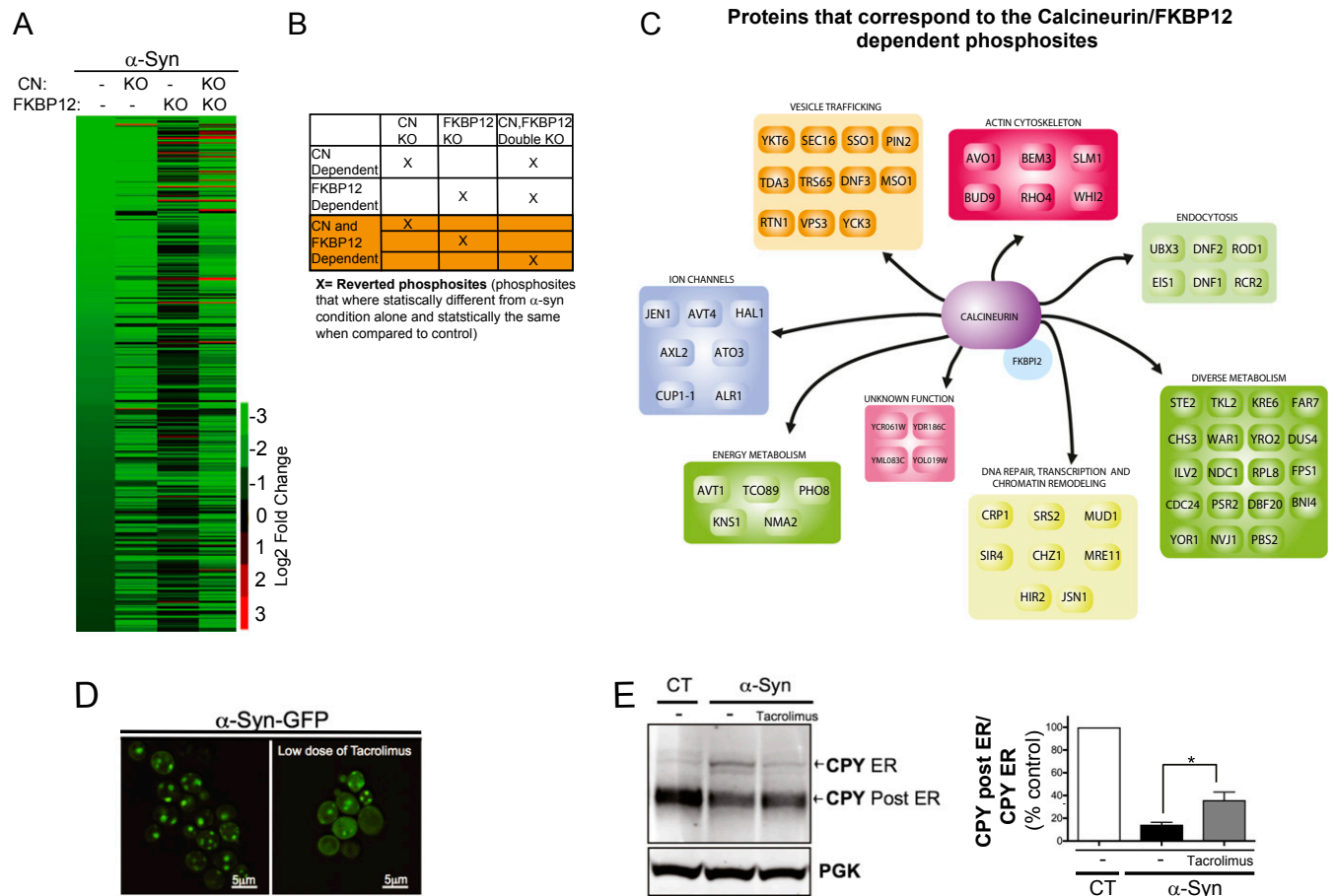
www.manaraa.com

Fig. 3. FKBP12 modulates calcineurin (CN) activity by altering its phospho-dependent proteome. (*A*) Heat map representing 527 hypophosphorylated phosphosites with abundances based on an MS shotgun approach. Cutoff was a |log2 FC| > 2 and *q* value < 0.05 between control and α-syn–expressing yeast cells across the different conditions. All of the Excel sheets associated with the data are available as tables in Dataset S1. (*B*) Diagram exemplifying how the CN- and FKBP12-dependent phosphosites were chosen. (*C*) Diagram of the proteins that contain all of the reverted CN/FKBP12-dependent phosphosites. Functions are annotated according to the SGD. (*D*) α-Syn–GFP localization in yeast cells in the presence (*D*, *Right*) and absence (*D*, *Left*) of protective dose of Tacrolimus (30 μg/mL). (*E*, *Left*) Western blot for CPY in α-syn–expressing cells in the presence and absence of a protective dose of Tacrolimus (30 μg/mL). Higher-molecular weight band represents the glycosylated form of CPY, which is typically found in the ER. The lower-molecular weight band (post-ER) is deglycosylated CPY, which has moved beyond the ER through the secretory pathway. Phosphoglycerate kinase (PGK) is used as a loading control. (*E*, *Right*) Quantitation of the ER and post-ER CPY bands from the Western blot; bands were quantitated using the Odyssey software. *P* < 0.05 (one-way ANOVA, Dunnett's multiple comparison test).

against α-syn toxicity. To test this hypothesis, we performed a phosphoproteomic analysis of yeast cells expressing empty vector (control), α-syn alone, and α-syn in cells deleted for (*i*) calcineurin, (*ii*) FKBP12, or (*iii*) both calcineurin and FKBP12 (Fig. 3*A*). Using a label-free approach, we quantified 13,641 phospho-peptides across all five conditions after normalizing for protein abundance (*Materials and Methods* has complete details). To detect differentially phosphorylated peptides, we compared control and α-syn–expressing yeast cells. We focused on those peptides showing at least a twofold (log2) change in abundance with a false discovery rate-adjusted *P* value (*q* value) < 0.05 (Fig. 3*A* and Fig. S3). These phosphopeptides were further annotated into unique phosphosites. For example, a given phosphopeptide could have multiple specific phosphorylation sites; hence, the data are reported as unique phosphosites within a given protein. Phosphorylation sites passing these criteria numbered 5,250.

Since calcineurin is a phosphatase highly activated in α-syn–expressing yeast cells, we concentrated our analysis on the two-fold hypophosphorylated subset (527 of 5,250) to define phosphosites that may be dephosphorylated by calcineurin. We reasoned that any hypophosphosites that gained phosphorylation in the α-syn yeast-expressing cells with the calcineurin deletion

are potentially calcineurin-dependent phosphosites. Likewise, if FKBP12 contributes to α-syn toxicity by enabling calcineurin to dephosphorylate specific substrates, then hypophosphosites that gained phosphorylation in the absence of FKBP12 should be similar and/or sensitive to the absence of calcineurin. The criteria for gain of phosphorylation (i.e., reversion) were established as those hypophosphosites with phosphorylation status that did not significantly change compared with the empty vector negative control cells (i.e., non–α-syn–expressing) but with status that was significantly more phosphorylated in the positive control α-syn–expressing cells. Based on this stringent test, the phosphosites that reverted were scored as positive for two thresholds and annotated as putative calcineurin-dependent phosphosites (Fig. 3*B* and Fig. S3).

In the calcineurin KO, ~4% of all of the hypophosphorylated sites satisfied the reversion criteria (Fig. 3*A* and Dataset S1). Strikingly, deletion of the yeast FKBP12 had a more profound effect on phosphorylation than deletion of calcineurin alone. When FKBP12 was deleted, ~34% of all of the hypophosphorylated sites fulfilled the reversion criteria. A minimal subset of these phosphosites was not affected by the absence of calcineurin and hence, is unique to the deletion of FKBP12 (Fig. 3*A*, Dataset S1, and Fig. S3). However, most of the phosphosites that reverted

Caraveo et al.

www.manaraa.com

to control in the FKBP12 KO strain were dependent on calcineurin, given that the reversion was lost in the double-KO strain of calcineurin and FKBP12 (Fig. 3*A* and Fig. S3).

To establish which of these phosphosites are dependent on the functional interaction of calcineurin and FKBP12, we focused on those with (*i*) reversion pattern that was shared between the calcineurin KO, FKBP12 KO, and the double-KO strains and (*ii*) reversion pattern in the single-KO strain that was either lost or gained in the double-KO strain (Fig. 3*B*). With these criteria, we retrieved 175 of 527 unique calcineurin- and FKBP12-dependent phosphosites that were subsequently mapped to their corresponding proteins, representing a list of 66 putative calcineurin- and FKBP12-dependent substrates (Fig. 3*C*). The canonical calcineurin substrate docking site LxVP can determine calcineurin substrate recognition (2). Within the 66 putative calcineurin and FKBP12-dependent substrates, we found a 2.3-fold enrichment for LxVP-containing motif proteins, further supporting their reliance on calcineurin ($P = 0.036$) (Dataset S2). Notably, these 66 substrates, one-half of which have human homologs, are within biological processes, which have been shown to be critical in the pathobiology of α-syn (25). Examples include YKT6 and YCK3 (16) in vesicle trafficking, SLM1 (2) in actin cytoskeleton organization, PBS2 (26) in mitochondrial function, and TC089 (27) and NMA2 (28) in aging and energy metabolism.

It is known that toxic levels of α-syn impair vesicle trafficking, resulting in the aggregation of α-syn into functionally diverse large vesicles readily visualized as foci (16, 17). If it is true that FKBP12 enables calcineurin-dependent dephosphorylation of substrates, which impairs vesicle trafficking, we reasoned that low doses of Tacrolimus should restore the block in vesicle trafficking caused by α-syn. Indeed, low doses of Tacrolimus reduced these α-syn–induced vesicle foci (Fig. 3*D*). An alternative way to assess vesicle trafficking defects is by following the mobility on a gel of the carboxypeptidase Y (CPY), the best studied soluble protein targeted to the vacuole (29). The block from endoplasmic reticulum (ER)–Golgi caused by α-syn causes an accumulation of the glycosylated form of CPY in the ER as manifested by its higher mobility in an acrylamide gel (Fig. 3*E*). Importantly, low protective doses of Tacrolimus restored the trafficking of CPY from the ER to the secretory pathway.

Taken together, these data coupled to the MS phosphoproteomic studies strongly support an endogenous functional interaction between FKBP12 and calcineurin, whereby FKBP12 has the ability to alter the calcineurin-dependent phosphoproteome toward proteins involved in vesicle trafficking, endocytosis, and actin cytoskeletal organization among other functional ontologies.

Subsaturating Doses of Tacrolimus Protect Against α-Syn Toxicity in Vivo. Our findings thus far establish a central role of FKBP12 in contributing to α-syn toxicity through at least two mechanisms: (*i*) by shifting the calcineurin-dependent phosphoproteome toward proteins involved in vesicle trafficking, endocytosis, actin cytoskeleton organization, etc. and (*ii*) by affecting other pathways independent of calcineurin, which have been previously implicated by other groups (24). Importantly, both of these toxic properties of FKBP12 can be pharmacologically rescued with low subsaturating doses of Tacrolimus. Our data suggest that subsaturating doses of Tacrolimus are key to maintain a minimal but essential level of calcineurin activity, which is critical to engage the potential protective substrates described above, while at the same time, inhibiting FKBP12 through a calcineurin-independent manner.

To investigate whether the protective properties of low doses of Tacrolimus are relevant in vivo, we turned to a rat model of PD. This model is based on unilateral stereotactic injection of an adeno-associated virus encoding α-syn directly into the substantia nigra pars compacta (SNc), a brain region highly affected in PD. Importantly, α-syn–induced damage in the SNc is reflected in the striatum, the region of the brain that receives all of the projections

from the dopaminergic neurons in the SNc. These defects include loss of DAT, loss of DA, and increases in DA's breakdown products, such as homovanillic acid (HVA) and 3,4-Dihydroxyphenylacertic acid (DOPAC) (13). The dysregulation of trafficking of the DATs as well as DA secretion at presynaptic terminals are responsible for the behavioral deficits in these animals (13).

Using this rat in vivo model of PD, we tested whether inhibiting calcineurin and FKBP12 over a range of Tacrolimus doses could ameliorate any of the neurological defects caused by α-syn (Fig. 4*A*). Indeed, the lower doses but not the higher doses of Tacrolimus rescued the behavioral deficits caused by α-syn as assessed by a paw asymmetry assay (Fig. 4*B*). The restoration in behavioral deficits caused by α-syn overexpression was accompanied by a rescue in the deficits of DATs (Fig. 4*C*), DA (Fig. 4*D*), and DA breakdown products DOPAC and HVA at the striatal terminals (Fig. S4*A*). Importantly, like in cell culture experiments, the differences in calcineurin activation between control and α-syn–expressing neurons were not caused by differences in calcineurin expression but rather, calcineurin activity (Fig. S4*C*).

Normal functioning at these terminals is highly dependent on biological processes, such as vesicle trafficking, endocytosis, and actin reorganization, and largely regulated by phosphorylation (30). Therefore, it is reasonable to consider that low doses of Tacrolimus protect against α-syn toxicity by regulating the phosphorylation of proteins implicated in boosting vesicle trafficking at the terminals, thereby facilitating DA transport and secretion.

To explore whether low doses of Tacrolimus can restore the phosphorylation of calcineurin- and FKBP12-dependent substrates important for the regulation of vesicular traffic at SNc presynaptic striatal terminals, we utilized Tandem Mass Tags (TMT) MS (31). This unbiased isobaric mass method allows one to quantitate phosphopeptides across animals and conditions postlysis. We reasoned that this is the best available approach, despite the fact that significant changes in the phosphorylation state of substrates at the SNc terminals would be masked by the rest of the other neuronal types present in the striatum, which are unaffected by α-syn. Despite these limitations, we detected 51 of 3,526 phosphopeptides that significantly changed comparing control and α-syn animals. Of these, one-half were significantly hypophosphorylated in the α-syn animals. We retrieved four phosphosites, two from each of two presynaptic proteins, with phosphorylation that increased in the animals treated with low doses of Tacrolimus (Fig. 4*E* and Dataset S3). Specifically, these proteins are GAP-43 and BASP1. Both proteins have critical roles in assisting neuronal path finding and branching during regeneration and contribute to presynaptic changes leading to neurotransmitter release, endocytosis, and synaptic vesicle recycling (32, 33). Importantly, their activity has been shown to be affected by calcineurin, although the exact mechanism of regulation is not known (34, 35). While these proteins do not have homologs in yeast, they share common features with the putative calcineurin- and FKBP12-dependent proteins retrieved from the yeast model. Specifically, these substrates regulate processes linked to endocytic, vesicle trafficking, and actin cytoskeleton dynamics, and they also contain an unusually high number of prolines, making them an ideal substrate for *cys-trans* prolyl isomerases, such as FKBP12.

Together, these data support the findings in yeast that targeting the endogenous functional interaction between calcineurin and FKBP12 with subsaturating doses of Tacrolimus is neuroprotective. Specifically, low doses of Tacrolimus can inhibit a fraction of active calcineurin/FKBP12 complexes, thereby modulating the phosphorylation of proteins critically involved in the restoration of DAT trafficking and DA secretion at presynaptic terminals to ultimately ameliorate the behavioral deficits caused by α-syn in a rat model of PD.

Discussion

Using α-syn toxicity as a model system and using genetic, pharmacologic, biochemical, and phosphoproteomic tools, we showed that the calcineurin-dependent phosphoproteome is
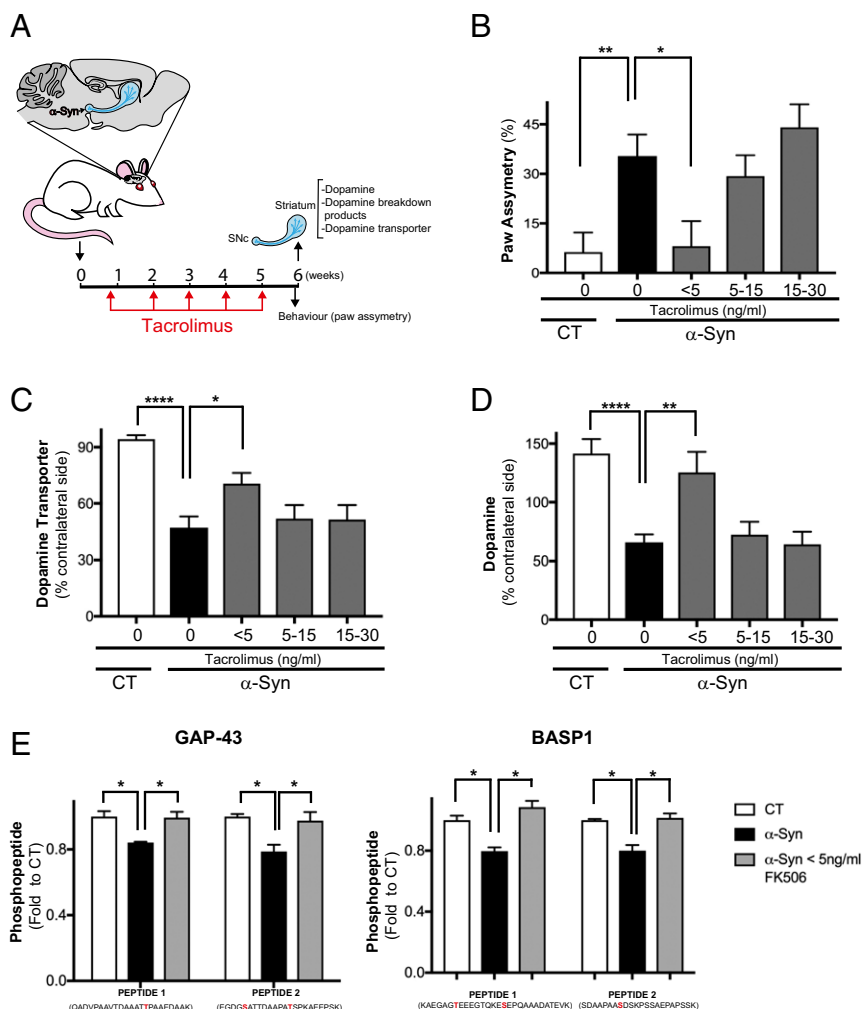
Fig. 4. Inhibition of calcineurin and FKBP12 by low doses of Tacrolimus protects against α-syn toxicity in vivo. (A) Diagram representing the rat in vivo experiment; briefly, $n = 25–30$ rats were injected unilaterally in the SNc with an AAV1/2 carrying either A53T α-syn or empty vector (CT). Four days after injection, rats were treated with different s.c. amounts of Tacrolimus on a weekly basis for 6 wk. Before the animals were killed, (B) the behavioral test for paw asymmetry was performed. Subsequently, striatal neurochemistry was performed. $*P < 0.02$ (one-way ANOVA, Dunnett's multiple comparison test); $**P < 0.007$ (one-way ANOVA, Dunnett's multiple comparison test). (C) DAT assayed by autoradiography at the striatum and normalized to its non–α-syn–injected contralateral side. $*P < 0.03$ (one-way ANOVA, Dunnett's multiple comparison test); $****P < 0.0001$ (one-way ANOVA, Dunnett's multiple comparison test). (D) DA measured by HPLC. $**P < 0.0016$ (one-way ANOVA, Dunnett's multiple comparison test); $****P < 0.0001$ (one-way ANOVA, Dunnett's multiple comparison test). (E) Striatal samples from CT, α-syn, and α-syn with <5 ng/mL of Tacrolimus were subjected to TMT MS (Materials and Methods), and phosphopeptides that were significantly rescued by Tacrolimus are shown. These phosphosites belong to two proteins: GAP-43 and BASP1. The phosphorylation site identified is highlighted in red. $n = 3$ rats. $*P < 0.05$ (two-tailed t test).

physiologically modulated by FKBP12. We found that the endogenous functional interaction between calcineurin and FKBP12 is associated with α-syn toxicity in that it leads to dephosphorylation of proteins involved in vesicle trafficking, endocytosis, and actin cytoskeletal organization among other functional ontologies. While neurons in general rely heavily on these processes for proper neurotransmitter release, DA neurons in the SNc might be particularly sensitive to these pathways given their high dependence on Ca^{2+} to drive tonic firing (36). Moreover, the additional contribution of α-syn to cytosolic Ca^{2+} will lead to a chronic activation of calcineurin/FKBP12 driving constitutive dephosphorylation of proteins, such as GAP-43 and BASP1. Improper regulation of these presynaptic proteins would manifest in deficits in the DAT at the plasma membrane and hence, DA release. This will, in turn, lead to cell death and the behavioral deficits observed in the disease (Fig. S5 A and B).

Questions arise as to how FKBP12 affects the calcineurin-dependent phosphoproteome. Can FKBP12 interact with calcineurin in conditions other than α-syn toxicity? Is the physiological interaction between calcineurin and FKBP12 only found under conditions of pathological Ca^{2+} dysregulation? Given that Tacrolimus can inhibit calcineurin under a variety of cell types and conditions, it would suggest that FKBP12 can regulate calcineurin activity under diverse circumstances and that the natural compound simply harnesses this endogenous interaction. Mechanistically, one possibility for FKBP12 effects on the calcineurin-dependent phosphoproteome evokes a role for FKBP12 in regulating the high-order structure of calcineurin and maintaining the holoenzyme in an active state. Indeed, the N-terminal region of calcineurin contains many prolines that could be isomerized by FKBP12 to retain an active conformation (37). Alternatively, FKBP12 could affect calcineurin's substrates. Intriguingly, all of the substrates that we retrieved contain either a high number of prolines or the consensus proline-containing calcineurin docking motif LxVP. Future research is required to elucidate these important mechanistic insights.

We previously reported that a tunable response to calcineurin with Tacrolimus, in response to α-syn toxicity, could rebalance the phosphatase activity—driving it away from a toxic pathway and toward a protective one (2). Our findings shed light on the plausible mechanism for this fine adjustment of calcineurin activity: low doses of Tacrolimus restore the phosphorylation of a subset of proteins that are dephosphorylated by calcineurin/FKBP12, which is necessary to achieve survival under α-syn toxicity (Fig. S5C). Importantly, the protective effects of low doses of Tacrolimus in the rat model of PD show that the control of FKBP12 over calcineurin activation, although first uncovered in yeast, is conserved in vivo in mammalian neurons. These findings reconcile a long-standing discrepancy regarding the role of the immunophilins, such as FKBP12, in PD. This is particularly relevant given that Tacrolimus was previously shown to have neuroprotective properties in mammalian PD models (38–40). Because other compounds that targeted immunophilins without affecting calcineurin function prevented neurodegeneration in specific animal models (41, 42), it was thought that Tacrolimus' protective effects were mediated solely through FKBPs. However, these same compounds failed to reverse PD motor symptoms in humans (43). Our findings establish that FKBP12 plays key roles in α-syn toxicity by affecting calcineurin-dependent and calcineurin-independent pathways. It is the partial inhibition of the calcineurin- and FKBP12-dependent pathways that was previously missed, and it can only be achieved with low doses of Tacrolimus. High doses of Tacrolimus are widely used in the clinic to suppress the rejection of organs in transplant patients, a process in which calcineurin also plays a critical role. Our insights into the mechanism of calcineurin/FKBP12 activation and hence, dosing of Tacrolimus provide a strong rationale for repurposing this drug against synucleinopathies, such as PD.

Materials and Methods

Mammalian Constructs. All neuronal constructs were cloned into the pLENTI6/V5 DEST (Invitrogen) lentivirus expression vector using the Gateway system. These included the genetic-encoded β-gal (LacZ) and α-syn A543T.

Rat Primary Cortical Cultures. Cultures were prepared based on Lesuisse and Martin (44). Embryos were harvested by Cesarean section from anesthetized pregnant Sprague–Dawley rats at embryonic day 18. Cerebral cortices were isolated and dissociated with ACCUMAX digestion for 20 min at 37 °C and trituration with Pasteur pipettes. Polyornithine- and laminin-coated 96-well plates were seeded with 4×10^4 cells in neurobasal medium (Life Technologies) supplemented with B27 (Life Technologies), 0.5 mM glutamine, 25 μM β-mercaptoethanol, penicillin (100 IU/mL), and streptomycin (100 μg/mL). One-third of the medium was changed every 3–4 d. Tacrolimus (Ontario Chemicals) and CsA (Sigma) at the indicated concentrations were added to the lentivirus-transduced cultures in 96-well plates at day in vitro 18 (DIV18), keeping the amount of DMSO constant (vehicle). As a surrogate marker of cell viability, cellular ATP content was measured using the ViaLight Plus kit (Lonza). Lentiviral constructs were packaged via lipid-mediated transient transfection of the expression constructs and packaging plasmids (pMD2.G and psPAX2) into 293 cells. Lentivirus were purified and concentrated using the Lenti-X Maxi Purification kit and LentiX Concentrator (Clontech) according to the manufacturer's protocol. Lentivirus titer was determined using the QuickTiter Lentivirus titer kit (lentivirus-associated HIV p24; Cell Biolabs) according to the manufacturer's protocol. Rat cortical cultures were transduced with high multiplicity of infection (25) or low (15) of lentivirus at DIV5.

Yeast Deletions. All deletions were performed by homologous recombination according to the Saccharomyces Genome Deletion Project using a one-step gene disruption. Briefly, a PCR-based strategy was performed to amplify a product that contains an antibiotic resistance cassette (either kanamycin or hygromycin) flanked by 45 bp of sequence corresponding to the 5′ and 3′ UTRs of the target gene (sequence available at the Saccaromyces Genome Deletion Project). Yeast strains were transformed with the PCR product using a standard lithium acetate protocol, allowed to recover overnight in yeast extract-peptone-dextrose media at 30 °C, and then, selected on plates with the corresponding antibiotic-resistant marker. Colonies were screened for the deletion using PCR confirmation primers. Results are representative of at least three independent colonies. All transformations in yeast for de-

letion purposes were performed at least three independent times and analyzed with at least three independent transformants each time.

Spotting Assays. Cells were grown overnight at 30 °C in 3 mL synthetic dropout (SD) medium lacking the relevant amino acids and containing glucose. Cell concentrations (OD_{600}) were adjusted to the lowest concentration, and then, they were fivefold serially diluted and spotted onto SD medium plates containing glucose (uninduced) or galactose (induced). Plates were incubated at 30 °C for 2 d (glucose) or 3 d (galactose).

MS Shotgun Approach.
Protein extraction from cell pellets. Dry cell pellets were resuspended in cell lysis buffer (8 M urea, 0.05 M ammonium bicarbonate, 0.005 M EDTA). Acid-washed glass beads (Sigma) were added at a 2:1 ratio with the cell pellet volume. Cells were disrupted with four cycles of 60 s of shaking in a FastPrep FP120 (MP Biomedicals) kept at 4 °C. Protein extract was collected, and concentration was assessed by BCA assay (Thermo Scientific) according to the manufacturer's instructions.
Protein digestion. To prepare samples for phosphopeptide abundance measurements, 4 mg of total protein from each extract was used for digestion. To prepare samples for protein abundance measurements, 250 μg of each extract was used. Disulfide bonds were reduced and alkylated with 10 mM Tris(2-carboxyethyl)phosphine for 1 h at 37 °C and 40 mM iodoacetamide for 1 h at 25 °C in the dark, respectively. Samples were diluted with 0.1 M ammonium bicarbonate to a concentration of 6 M urea, and lysyl endopeptidase (MS grade; Wako Pure Chemical Industries) was added to a final enzyme:substrate ratio of 1:100. Samples were incubated at 37 °C for 3 h and then, further diluted to a final concentration of 1.5 M urea; sequencing-grade porcine trypsin (Promega) was added to a final enzyme:substrate ratio of 1:100. Tryptic digestion was conducted overnight at 30 °C. The digestion was stopped by acidification with formic acid to 2%. The peptide mixtures were loaded onto Sep-Pak tC18 cartridges (Waters), desalted, and eluted with 80% acetonitrile (ACN). Peptide samples were evaporated on a vacuum centrifuge and stored dry at −20 °C.
Phosphopeptide enrichment. Four-milligram protein digests were enriched for phosphopeptides by titanium dioxide (TiO₂) chromatography. Peptides were reconstituted in a solution of 80% can and 6% TFA. Solubilized peptides were added to TiO₂ resin (GL Science) at a ratio of 1 mg peptide:1 mg TiO₂ resin, and samples were incubated for 1 h with end-over-end rotation. The resin was washed with a solution of 80% ACN and 6% TFA; then, it was washed with a 50% ACN, 0.1% TFA, and 0.2 M NaCl solution and a 50% ACN and 0.1% TFA solution. Phosphopeptides were eluted twice with 5% NH₄OH. The pH was rapidly adjusted to pH < 3 using 100% TFA. Phosphopeptides were purified using Sep-Pak tC18 cartridges (Waters) as described above. Dried phosphopeptides were resolubilized with 30 μL 0.1% formic acid before analysis by MS.
Relative phosphopeptide quantification by label-free shotgun proteomics. Peptide and phosphopeptide samples for protein abundance and phosphopeptide abundance measurements, respectively, were separately analyzed by liquid chromatography (LC)-MS/MS on a Q-Exactive plus (QE+) mass spectrometer (Thermo Scientific) equipped with a nanoelectrospray ion source. Online chromatographic separation of the peptides was conducted by an EASY nanoliquid chromatography system (Proxeon) equipped with a 40-cm fused silica column with a 75-μm i.d. (New Objective); peptides were packed with Reprosil Pur C18 Aq 1.9-μm beads (Dr. Maisch) and heated to 50 °C. The peptide mixtures (2 μL) were separated with a linear gradient from 5 to 35% ACN in 120 min at 0.3 μL/min. Precursor scans were performed at a resolution of 70,000 at 200 m/z. After each precursor scan, 20 MS/MS spectra were acquired after high-energy collisional dissociation in the Orbitrap at a resolution of 17,500 at 200 m/z. The intensity threshold for peptide fragmentation was set to 3.6e4, and a dynamic exclusion window of 30 s was used. The collected spectra were searched using Sequest HT against the *Saccharomyces cerevisiae* Saccharomyces Genome Database (SGD) protein database with Proteome Discoverer (version 1.4; Thermo Scientific). Trypsin was set as the digesting protease with the tolerance of two missed cleavages and semitryptic termini. The monoisotopic peptide and fragment mass tolerances were set to 10 ppm and 0.02 Da, respectively. Carbamidomethylation of cysteines (+57.0214 Da) was defined as a fixed modification, and oxidation of methionines (+15.99492 Da) was defined as a variable modification. Phosphorylation of serines, threonines, or tyrosines (+79.966 Da) was defined as variable modifications when searching the phosphopeptide-enriched samples. Peptide spectrum matches were filtered using Percolator at a false discovery rate of 1%, determined using a reverse sequence decoy database.

Raw data were imported into Progenesis QI (Nonlinear dynamics) for MS analyzer 1 (MS1) feature alignment, normalization, and matching of peptide identifications (described above) to the accurate m/z and retention time of MS1 features. The area under the extracted ion chromatograms of all identified MS1 features (peptide ions) was exported. Individual phosphopeptide measure-

Caraveo et al.

www.manaraa.com

ments were scaled applying the protein-level data using the median of protein abundance between biological triplicates. Peptides for which the protein abundance measurement was missing or was not univocally determined were excluded from the analysis. The R-based SafeQuant package (45) (version 1.1) was used for normalization, quantification, and statistical analysis between samples. Phosphopeptide abundance ratios between conditions and control or HiTox samples with their associated q values (P values adjusted for multiple testing) were calculated (Dataset S1, raw_data_refControl and raw_data_refHiTox sheets). Nonphosphorylated peptides were next filtered out, and a q-value cutoff of 0.05 was applied to the remaining ones. Finally, phosphorylated peptides referring to the same modification were grouped: this allowed for the assignment of a unique fold change (FC) for each unique phosphosite. The FC was calculated as the mean of all of the FCs measured for the same phosphosite. To statistically assess the combination of the q values, a Fisher's combined probability test was applied to combine q values (Dataset S1, Cleaned_Table_refControl and Cleaned_Table_refHitox sheets). These datasets were used to identify phosphosites, which reverted to control, using the criteria described in the result session.

TMT MS.

Reduction, alkylation, and tryptic digestion. Cells were lysed in 8 M urea (Sigma) and were quantified using BCA assay (Pierce). Proteins were reduced with 10 mM DTT (Sigma) for 1 h at 56 °C and then alkylated with 55 mM iodoacetamide (Sigma) for 1 h at 25 °C in the dark. Proteins were then digested with modified trypsin (Promega) at an enzyme:substrate ratio of 1:50 in 100 mM ammonium acetate, pH 8.9, at 25 °C overnight. Trypsin activity was halted by the addition of acetic acid (99.9%; Sigma) to a final concentration of 5%. After desalting using a C18 Sep-Pak Plus cartridge (Waters), peptides were lyophilized in 400-µg aliquots and stored at −80 °C.

TMT labeling. Peptide labeling with TMT 6plex (Thermo) was performed per the manufacturer's instructions. Lyophilized samples were dissolved in 70 µL ethanol and 30 µL of 500 mM triethylammonium bicarbonate, pH 8.5, and the TMT reagent was dissolved in 30 µL of anhydrous ACN. The solution containing peptides and TMT reagent was vortexed and incubated at room temperature for 1 h. Samples labeled with the 10 different isotopic TMT reagents were combined and concentrated to completion in a vacuum centrifuge.

Peptide fractionation. The TMT-labeled peptide pellet was fractionated via high-pH reverse-phase HPLC. Peptides were resuspended in 100 µL buffer A [10 mM triethylammonium bicarbonate (TEAB), pH 8] and separated on a 4.6 × 250-mm 300 Extend-C18, 5-µm column (Agilent) using an 90-min gradient with buffer B (90% MeCN, 10 mM TEAB, pH 8) at a flow rate of 1 mL/min. The gradient was as follows: 1–5% B (0–10 min), 5–35% B (10–70 min), 35–70% B (70–80 min), and 70% B (80–90 min). Fractions were collected over 75 min at 1-min intervals from 10 to 85 min. The fractions were concatenated into 15 fractions noncontiguously (1 + 16 + 31 + 46 + 61, 2 + 17 + 32 + 47 + 62, etc.). The fractions were speed-vacuumed (Thermo Scientific Savant) to near dryness.

Phosphopeptide enrichment. Phosphopeptides were enriched from each of the 15 fractions using the High-Select Fe-NTA phosphopeptide enrichment kit (Thermo) per the manufacturer's instructions.

LC-MS/MS. Peptides were loaded on a precolumn and separated by reverse-phase HPLC using an EASY-nLC1000 (Thermo) over a 140-min gradient before nano-electrospray using a QExactive Plus mass spectrometer (Thermo). The mass spectrometer was operated in a data-dependent mode. The parameters for the full-scan MS were resolution of 70,000 across 350–2,000 m/z, automatic gain control target, 3e6 ion counts, and maximum inverted terminal repeats 50 ms. The full MS scan was followed by MS/MS for the top 10 precursor ions in each cycle with an normalized collision energy of 34 and dynamic exclusion of 30 s. Raw mass spectral data files (.raw) were searched using Proteome Discoverer (Thermo) and Mascot, version 2.4.1 (Matrix Science). Mascot search parameters were 10-ppm mass tolerance for precursor ions, 15 milli mass units for fragment ion mass tolerance, and two missed cleavages of trypsin. Fixed modifications were carbamidomethylation of cysteine and TMT 10plex modification of lysines and peptide N termini; variable modifications were methionine oxidation, tyrosine phosphorylation, and serine/threonine phosphorylation. TMT quantification was obtained using Proteome Discoverer, isotopically corrected per the manufacturer's instructions, and normalized to the mean of each TMT channel. Only peptides with a Mascot score greater than or equal to 25 and an isolation interference less than or equal to 30 were included in the data analysis.

Rat in Vivo Studies.

Animals and surgery. Using standard stereotaxic procedures, 60 female Sprague–Dawley rats (~280 g; Charles River) were injected intranigrally with either empty adeno-associated vector 1/2 (AAV1/2) vector or AAV1/2 expressing human A53T α-syn under isoflurane/oxygen anesthesia. In each case, a single 2-µL injection of viral vector was delivered to the substantia nigra at a rate of

0.5 µL/min according to the following coordinates from bregma: anterior/posterior, −5.2 mm; mediolateral, −2.0 mm; dorsoventral, −7.5 mm (from skull at bregma) using a microinjector (Stoelting) and according to the atlas of Paxinos and Watson (46). The AAV1/2 concentration for each vector was 5.2 × 10 exp12 genomic particles per 1 mL. Animals were housed in pairs in a temperature-controlled environment (20 µC), kept on a regular 12-h light/dark cycle (lights on 0630 hours), and allowed food and water ad libitum. After 3 wk postsurgery, animals were euthanized for additional analysis. All procedures were conducted under an approved Institutional Animal Care and Use Committee (University Health Network, protocol 1738, in accordance with the guidelines and regulations set by the Canadian Council on Animal Care).

Vectors. AAVs of a 1/2 serotype were designed such that expression was driven by a chicken beta actin (CBA) promoter hybridized with the CMV immediate early-enhancer sequence. In addition, a woodchuck posttranscriptional regulatory element (WPRE) and a bovine growth hormone polyadenylation sequence were incorporated to further enhance transcription after transduction. AAV1/2 is a chimeric vector, where the capsid expresses AAV1 and AAV2 serotype proteins in a 1:1 ratio and uses the inverted terminal repeats from AAV2 according to the following scheme: CMV/CBA promoter––human A53T α-syn. The vectors were produced by GeneDetect Ltd.. Viral titers were determined by qPCR (Applied Biosystems 7900 QPCR) with primers directed to the WPRE region, thus representing the number of functional physical particles of AAV in the solution containing the genome to be delivered. Full details of vector design can be found in ref. 13.

Tacrolimus dosing. Rats (n = 25–30) were injected with either 1 or 0.2 mg/kg of Tacrolimus s.c. 4 d after surgery and every 8 d after that. Tacrolimus was formulated in 5% DMSO, 7.5% cremophor EL, and 87.5% PBS. Injection volume was 500 µL for an average weight of 320 g per rat.

Tacrolimus determination in the brain. Tacrolimus content was determined in the rat cortex using liquid chromatography–MS by Sanford Burnham.

Brain processing. At 3 wk postvirus injection, animals received an overdose of pentobarbital (i.p.) and were killed by exsanguination by way of transcardial perfusion with ice-cold 0.9% saline containing 0.2% heparin. Brains were then placed ventral up into an ice-cold stainless steel rat brain matrix and cut in the coronal plane at the level of the optic chiasma. The rostral portion of the brain, including the anterior striatum, was immediately frozen in isopentane chilled to −42 °C for the quantification of levels of DAT by autoradiography. A 1-mm coronal slice was then made to the remaining brain in the tissue matrix, and from this, striatum was fresh dissected and placed into Eppendorf tubes for preparation to assess DA and metabolites of DA (HVA and DOPAC) by HPLC. The remainder of the caudal portion of the brain, including the mesencephalon, was immersed in 4% paraformaldehyde for 48 h for fixation followed by cryoprotection in graded sucrose solutions (15–30% sucrose). Tissue prepared in this manner was used for immunohistochemistry of tyrosine hydroxylase. HPLC striatal dissections were homogenized in 200 µL of 0.1 M TCA, which contained 10^{-2} M sodium acetate, 10^{-4} M EDTA, and 10.5% methanol (pH 3.8), using a tissue dismembrator (Fisher Scientific). Samples were spun in a microcentrifuge at 10,000 × g for 20 min. The supernatant was removed and stored at −80 °C. The pellet was used for total protein content analysis. Supernatant was thawed and spun for 20 min. Catecholamines were determined by a specific HPLC assay utilizing an Antec Decade II (oxidation: 0.5) electrochemical detector operated at 33 °C. Samples of the supernatant were injected using a Waters 717+ autosampler onto a Phenomenex Nucleosil (5 µm, 100 A) C18 HPLC column (150 × 4.60 mm). Analytes were eluted with a mobile phase consisting of 89.5% 0.1 M TCA, 10^{-2} M sodium acetate, 10^{-4} M EDTA, and 10.5% methanol (pH 3.8). Solvent was delivered at 0.8 mL/min using a Waters 515 HPLC pump. Using this HPLC solvent, analytes were observed in the following order: DOPAC, DA, and HVA. HPLC control and data acquisition were managed by Waters Empower software. Total protein for each sample was determined using the Peirce BCA protein assay (BCA assay; Pierce). Values of catecholamines are expressed as nanograms of analyte per milligram total protein.

DAT binding. The levels of striatal DAT were assessed by [125I]-RTI-121 binding autoradiography in cryostat-cut sections prepared from 20 µm fresh-frozen tissue. Briefly, thawed slides were placed in binding buffer (2 × 15 min, room temperature) containing 50 mM Tris, 120 mM NaCl, and 5 mM KCl. Sections were then placed in the same buffer containing 50 pM [125I]-RTI-121 (specific activity 2,200 Ci/µmol; Perkin-Elmer) for 120 min at 25 °C to determine total binding. Nonspecific binding was defined as that observed in the presence of 100 µM GBR 12909 (Tocris Bioscience). All slides were then washed (4 × 15 min) in ice-cold binding buffer, rinsed in ice-cold distilled water, and air-dried. Together with [125I]-microscale standards (Amersham), slides were then apposed to autoradiographic film (Kodak) and left for ~7 d at room temperature before developing. Autoradiograms were then analyzed using MCID

Caraveo et al.

software (Image Research Inc.). Densitometric analysis of three striata from each animal was carried out, whereby a reference curve of cpm vs. OD was calculated from β-emitting [^{14}C] microscale standards and used to quantify the intensity of signal as nanocuries per gram. Background intensity was subtracted from each reading. Data were then expressed as mean ± SEM signal intensity for each treatment group. Nonspecific binding was calculated in the same way and subtracted from the total to give specific binding. Nonspecific binding is typically found to account for <1% of total binding.

Motif Enrichment Analysis. ORFs from the genome of the ScS288c strain containing LxVP, PxIxIT, or both patterns were identified using the Yeast Genome Pattern Matching tool provided by the SGD; for each list of phosphosites identified in a specific experimental condition, the corresponding list of ORFs was analyzed to obtain counts for ORFs containing LxVP, ORFs containing PxIxIT, and ORFs containing both patterns, respectively. Enrichment was cal-

culated as the percentage of ORFs containing each specific pattern (or both patterns) in the experimental list divided by the percentage of ORFs containing the same pattern(s) in all ORFs of the genome. P value for the null hypothesis (i.e., there is no enrichment) was calculated using Pearson's χ^2 test.

1. Rusnak F, Mertz P (2000) Calcineurin: Form and function. *Physiol Rev* 80:1483–1521.
2. Caraveo G, et al. (2014) Calcineurin determines toxic versus beneficial responses to α-synuclein. *Proc Natl Acad Sci USA* 111:E3544–E3552.
3. Martí MJ, Tolosa E, Campdelacreu J (2003) Clinical overview of the synucleinopathies. *Mov Disord* 18(Suppl 6):S21–S27.
4. Hurwitz MY, Putkey JA, Klee CB, Means AR (1988) Domain II of calmodulin is involved in activation of calcineurin. *FEBS Lett* 238:82–86.
5. Klee CB, Crouch TH, Krinks MH (1979) Calcineurin: A calcium- and calmodulin-binding protein of the nervous system. *Proc Natl Acad Sci USA* 76:6270–6273.
6. Liu J, et al. (1991) Calcineurin is a common target of cyclophilin-cyclosporin A and FKBP-FK506 complexes. *Cell* 66:807–815.
7. Shin DW, et al. (2002) Ca(2+)-dependent interaction between FKBP12 and calcineurin regulates activity of the Ca(2+) release channel in skeletal muscle. *Biophys J* 83:2539–2549.
8. Qiu Y, et al. (2014) FK506-binding protein 12 modulates μ-opioid receptor phosphorylation and protein kinase C(ε)-dependent signaling by its direct interaction with the receptor. *Mol Pharmacol* 85:37–49.
9. Cardenas ME, et al. (1994) Immunophilins interact with calcineurin in the absence of exogenous immunosuppressive ligands. *EMBO J* 13:5944–5957.
10. Dawson TM, et al. (1994) The immunophilins, FK506 binding protein and cyclophilin, are discretely localized in the brain: Relationship to calcineurin. *Neuroscience* 62:569–580.
11. Steiner JP, et al. (1992) High brain densities of the immunophilin FKBP colocalized with calcineurin. *Nature* 358:584–587.
12. Luo J, et al. (2014) A calcineurin- and NFAT-dependent pathway is involved in α-synuclein-induced degeneration of midbrain dopaminergic neurons. *Hum Mol Genet* 23:6567–6574.
13. Koprich JB, Johnston TH, Reyes MG, Sun X, Brotchie JM (2010) Expression of human A53T alpha-synuclein in the rat substantia nigra using a novel AAV1/2 vector produces a rapidly evolving pathology with protein aggregation, dystrophic neurite architecture and nigrostriatal degeneration with potential to model the pathology of Parkinson's disease. *Mol Neurodegener* 5:43.
14. Chung CY, et al. (2013) Identification and rescue of α-synuclein toxicity in Parkinson patient-derived neurons. *Science* 342:983–987.
15. Tardiff DF, et al. (2013) Yeast reveal a "druggable" Rsp5/Nedd4 network that ameliorates α-synuclein toxicity in neurons. *Science* 342:979–983.
16. Cooper AA, et al. (2006) Alpha-synuclein blocks ER-Golgi traffic and Rab1 rescues neuron loss in Parkinson's models. *Science* 313:324–328.
17. Outeiro TF, Lindquist S (2003) Yeast cells provide insight into alpha-synuclein biology and pathobiology. *Science* 302:1772–1775.
18. Su LJ, et al. (2010) Compounds from an unbiased chemical screen reverse both ER-to-Golgi trafficking defects and mitochondrial dysfunction in Parkinson's disease models. *Dis Model Mech* 3:194–208.
19. Roy J, Li H, Hogan PG, Cyert MS (2007) A conserved docking site modulates substrate affinity for calcineurin, signaling output, and in vivo function. *Mol Cell* 25:889–901.
20. Polymeropoulos MH, et al. (1997) Mutation in the alpha-synuclein gene identified in families with Parkinson's disease. *Science* 276:2045–2047.
21. Irwin DJ, et al. (2012) Neuropathologic substrates of Parkinson disease dementia. *Ann Neurol* 72:587–598.
22. Dolinski K, Muir S, Cardenas M, Heitman J (1997) All cyclophilins and FK506 binding proteins are, individually and collectively, dispensable for viability in Saccharomyces cerevisiae. *Proc Natl Acad Sci USA* 94:13093–13098.
23. Griffith JP, et al. (1995) X-ray structure of calcineurin inhibited by the immunophilin-immunosuppressant FKBP12-FK506 complex. *Cell* 82:507–522.
24. Gerard M, et al. (2010) Inhibition of FK506 binding proteins reduces alpha-synuclein aggregation and Parkinson's disease-like pathology. *J Neurosci* 30:2454–2463.
25. Auluck PK, Caraveo G, Lindquist S (2010) α-Synuclein: Membrane interactions and toxicity in Parkinson's disease. *Annu Rev Cell Dev Biol* 26:211–233.
26. Kim EK, Choi EJ (2010) Pathological roles of MAPK signaling pathways in human diseases. *Biochim Biophys Acta* 1802:396–405.
27. Das F, et al. (2011) High glucose upregulation of early-onset Parkinson's disease protein DJ-1 integrates the PRAS40/TORC1 axis to mesangial cell hypertrophy. *Cell Signal* 23:1311–1319.
28. Fu L, Doreswamy V, Prakash R (2014) The biochemical pathways of central nervous system neural degeneration in niacin deficiency. *Neural Regen Res* 9:1509–1513.
29. Feyder S, De Craene JO, Bär S, Bertazzi DL, Friant S (2015) Membrane trafficking in the yeast Saccharomyces cerevisiae model. *Int J Mol Sci* 16:1509–1525.
30. Tuck E, Cavalli V (2010) Roles of membrane trafficking in nerve repair and regeneration. *Commun Integr Biol* 3:209–214.
31. Dayon L, Sanchez JC (2012) Relative protein quantification by MS/MS using the tandem mass tag technology. *Methods Mol Biol* 893:115–127.
32. Denny JB (2006) Molecular mechanisms, biological actions, and neuropharmacology of the growth-associated protein GAP-43. *Curr Neuropharmacol* 4:293–304.
33. Korshunova I, et al. (2008) Characterization of BASP1-mediated neurite outgrowth. *J Neurosci Res* 86:2201–2213.
34. Kobayashi Y, et al. (2015) Ganglioside contained in the neuronal tissue-enriched acidic protein of 22 kDa (NAP-22) fraction prepared from the detergent-resistant membrane microdomain of rat brain inhibits the phosphatase activity of calcineurin. *J Neurosci Res* 93:1462–1470.
35. Madsen JR, et al. (1998) Tacrolimus (FK506) increases neuronal expression of GAP-43 and improves functional recovery after spinal cord injury in rats. *Exp Neurol* 154:673–683.
36. Chan CS, et al. (2007) 'Rejuvenation' protects neurons in mouse models of Parkinson's disease. *Nature* 447:1081–1086.
37. Guasch A, et al. (2015) Calcineurin undergoes a conformational switch evoked via peptidyl-prolyl isomerization. *PLoS One* 10:e0134569.
38. Costantini LC, et al. (1998) A novel immunophilin ligand: Distinct branching effects on dopaminergic neurons in culture and neurotrophic actions after oral administration in an animal model of Parkinson's disease. *Neurobiol Dis* 5:97–106.
39. Guo X, Dillman JF, 3rd, Dawson VL, Dawson TM (2001) Neuroimmunophilins: Novel neuroprotective and neuroregenerative targets. *Ann Neurol* 50:6–16.
40. Guo X, Dawson VL, Dawson TM (2001) Neuroimmunophilin ligands exert neuroregeneration and neuroprotection in midbrain dopaminergic neurons. *Eur J Neurosci* 13:1683–1693.
41. Armistead DM, et al. (1995) Design, synthesis and structure of non-macrocyclic inhibitors of FKBP12, the major binding protein for the immunosuppressant FK506. *Acta Crystallogr D Biol Crystallogr* 51:522–528.
42. Steiner JP, et al. (1997) Neurotrophic actions of nonimmunosuppressive analogues of immunosuppressive drugs FK506, rapamycin and cyclosporin A. *Nat Med* 3:421–428.
43. Meissner W, Hill MP, Tison F, Gross CE, Bezard E (2004) Neuroprotective strategies for Parkinson's disease: Conceptual limits of animal models and clinical trials. *Trends Pharmacol Sci* 25:249–253.
44. Lesuisse C, Martin LJ (2002) Long-term culture of mouse cortical neurons as a model for neuronal development, aging and death. *J Neurobiol* 51:9–23.
45. Choi H, Glatter T, Gstaiger M, Nesvizhskii AI (2012) SAINT-MS1: Protein-protein interaction scoring using label-free intensity data in affinity purification-mass spectrometry experiments. *J Proteome Res* 11:2619–2624.
46. Paxinos G, Watson C (2007) *The Rat Brain in Stereotaxic Coordinates* (Academic, San Diego).

www.manaraa.com